Kinetic Modeling of Methanol to Olefins Process Over SAPO-34 Catalyst Based on the Dual-Cycle Reaction Mechanism

Xiaoshuai Yuan [ORCID]

Dalian National Laboratory for Clean Energy, National Engineering Laboratory for MTO, Dalian Institute of Chemical Physics, Chinese Academy of Sciences, Dalian 116023, P.R. China

University of Chinese Academy of Sciences, Beijing 100049, P.R. China

Hua Li [ORCID]**, Mao Ye and Zhongmin Liu**

Dalian National Laboratory for Clean Energy, National Engineering Laboratory for MTO, Dalian Institute of Chemical Physics, Chinese Academy of Sciences, Dalian 116023, P.R. China

A kinetic model for methanol to olefins (MTO) process over SAPO-34 catalyst was established based on the dual-cycle reaction mechanism. Simplifications were made by assuming olefins-based cycle as virtual species S*, and aromatics-based cycle as* R*, where the former mainly accounts for the production of higher olefins, while the latter for lower olefins. Transformation of* S *to* R *was considered with the participation of methanol and olefins. Meanwhile, a phenomenological deactivation model was developed to account for the deactivation process. With the proposed model, the evolution of methanol conversion and product selectivity with time on stream could be predicted, and key reaction characteristics, such as the autocatalytic nature of the reaction, could also be captured due to its mechanism-based nature. Further simulations of MTO reactors at different scales validated the robustness and applicability of the current model in MTO process development and optimization.* © 2018 American Institute of Chemical Engineers *AIChE J*, 65: 662–674, 2019
Keywords: methanol to olefins, kinetic model, SAPO-34, deactivation

Introduction

The research of methanol to olefins (MTO) has made significant progresses since its discovery in the 1970s by researchers at Mobil Oil. A recent breakthrough is that the world's first commercial unit based on the DMTO technology, namely the MTO technology developed by the Dalian Institute of Chemical Physics (DICP), Chinese Academy of Sciences, was successfully started up in 2010.[1] Thereafter, MTO has become a robust and significant route for producing light olefins from nonoil resources. By the end of 2017, 12 DMTO units are in operation and the total production capacity of olefins is about 6.46 million metric ton per annum. Despite the prosperity in industrial applications, some key issues related to the MTO process remain nontrivial tasks for scientists and engineers. On the one hand, the reaction mechanisms such as the formation of the first C—C bond are still unknown. On the other hand, the detailed kinetic model based on the fundamental understanding of MTO reaction mechanism is highly desired in order to further optimize the reactor design and operation.

Reaction mechanism is the basis for kinetic modeling. In the early work, researchers found that there are some significant features in methanol conversion process, for example, the autocatalytic nature of the reaction,[2-4] and the existence of an induction period.[3,5,6] Thereafter, an indirect mechanism was proposed to account for the production of ethylene and higher alkenes.[7-10] Based on these researches, Dahl and Kolboe[11-13] proposed the hydrocarbon pool mechanism and suggested that the methanol conversion starts by the formation of active hydrocarbon pool species, and then methanol reacts with these species to produce ethylene, propylene, and other olefins. Olsbye et al.[14-16] further extended the hydrocarbon pool mechanism to the dual-cycle mechanism for the MTO reaction over H-ZSM-5 catalyst. They proposed that methanol conversion takes place simultaneously *via* an olefins-based cycle and an aromatics-based cycle, respectively: the olefins-based cycle only produces propylene and higher olefins, and the aromatics-based cycle produces ethylene and propylene. Dai et al.[17] investigated the MTO reaction over H-SAPO-34 catalyst, and suggested that an olefins-based cycle dominates the early stages of the reaction, and as the conversion proceedings, an aromatics-based cycle is also involved. Wang et al.[18,19] studied the dual-cycle mechanism for MTO process over SAPO-34 catalyst by use of the first principles density functional theory simulations, and established a full reaction network for this process. Their simulation results indicated that both the aromatics-based and olefins-based cycle run simultaneously over SAPO-34 catalyst, whereas the ethylene is mainly formed through the aromatics-based cycle. Based on the isotopic tracer experiments, Hwang et al.[20] concluded that the concepts of the dual cycle mechanism should be further

Correspondence concerning this article should be addressed to M. Ye at maoye@dicp.ac.cn and H. Li at lihua@dicp.ac.cn.

extended to methanol conversions over SAPO-34 catalyst. Nevertheless, a kinetic model considering the dual-cycle mechanism is of practical importance for MTO process development.

Various kinetic models have been established so far for MTO process, which could be roughly divided into two categories, that is, detailed kinetic models and lumped kinetic models. The detailed kinetic models are essential for reaction mechanism research and can also be used in catalyst design and development. Park and Froment[21,22] developed a detailed kinetic model for the MTO process over HZSM-5 catalysts based on elementary steps of carbenium ion chemistry. The proposed model includes 726 elementary steps and 225 reaction species. Based on the hydrocarbon pool mechanism, Kumar et al.[23] also proposed a detailed kinetic model for MTO process, which includes 318 elementary steps and 107 species. Although kinetic parameters are reduced significantly with the single event approach in these models, the huge number of reactions makes the detailed kinetic model hard to be implemented in the reactor design and operation optimization.

Based on the hydrocarbon pool mechanism, Bos et al.[24] introduced a lumped kinetic model for MTO reaction over SAPO-34 catalyst with 8 lumps and 12 reactions. By use of this model, Bos et al.[24] compared different reactor types for MTO processes, and found that fast fluidized bed reactor and turbulent fluidized bed reactor are suitable for the industrial applications. Later on, Gayubo et al.[25] simplified Bos' kinetic model and introduced a parameter to quantify the effect of water at each reaction step. To further consider the effect of induction period and deactivation in MTO process, Gayubo et al.[26,27] developed a kinetic model based on experiments with SAPO-18 catalyst, in which they considered the formation of active intermediates as well as catalyst activity. In a recent contribution, a seven lumped kinetic model was proposed based on experiments over the DMTO catalyst.[28] A lumped model is more appropriate for reactor design and operation optimization. However, the above-mentioned lumped models are oversimplified, and could not reflect the detailed reaction mechanism and need to be validated carefully.

Recently, Xiao et al.[29,30] proposed a lumped kinetic model consisting of 17 reactions and 15 species, in which light olefins are described separately to simulate their monolith methanol to propylene (MTP) reactor behavior. Wen et al.[31] established a kinetic model considering 19 reactions and 10 lumps to evaluate the MTP reaction over structured SS-fiber@HZSM-5 core-shell catalyst. Huang et al.[32,33] established a rigorous kinetic model based on the co-reaction of methanol and olefins, and applied to the optimization of olefin recycle in MTP process. In the above-mentioned kinetic models, the simplified reaction mechanism of MTP process was considered, which can provide more information regarding the formation of individual major products. Since the coke-induced deactivation is relatively slow in the MTP process, the formation of coke is usually ignored in the proposed models.

For MTO reaction over SAPO-34, however, the coke deposited on the catalyst is critical to methanol conversion and product selectivity, thus the time-dependent coking behavior cannot be ignored in the kinetic model. However, in the published kinetic models, the time-dependent coking behavior in the MTO process is not well represented. Wragg et al.[34] developed a simplified kinetic model based on the mechanistic
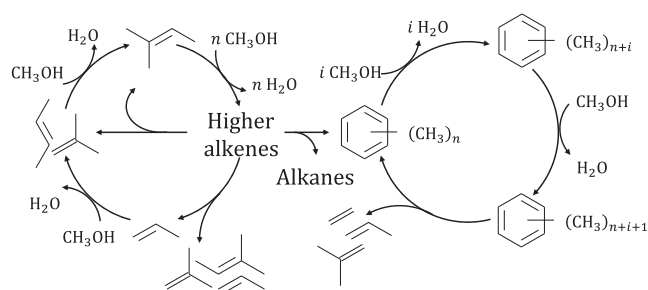
Figure 1. The dual-cycle mechanism for methanol conversion on ZSM-5. Reproduced from Ref. 36.

study of the induction period, aiming to reproduce the formation and evolution of the aromatic intermediates with time on stream. Since they only considered the formation of propylene, monocylic aromatics, and polyaromatic coke molecules, the proposed model was limited to mechanistic studies.

In this work, we attempt to develop a kinetic model for MTO process over SAPO-34 catalyst based on the detailed dual cycle mechanism, and a phenomenological model is proposed to account for the deactivation process of the catalyst. In this way, the time-dependent reaction behavior of the MTO process could be simulated, and the main reaction characteristics could also be captured. Thus, the model could be applied to the simulation of MTO reactors at different scales.

Reaction Kinetics

Reaction scheme

A realistic kinetic model should be developed on the basis of plausible reaction mechanisms, which provides detailed information about the reaction network and possible reaction routes. Recent studies suggest that products in methanol to hydrocarbons process are formed *via* a dual-cycle mechanism, which exhibits autocatalytic behavior.[14-20] However, most of the proposed kinetic models only consider the parallel reactions from methanol, which can be regarded as a simplified reaction network based on the hydrocarbon pool mechanism.[24-28,35] A kinetic model for MTO process based on the dual-cycle mechanism remains a challenge.

Figure 1 shows the scheme of the dual-cycle mechanism for MTO reaction over ZSM-5 catalyst.[36] This scheme can be extended to SAPO-34 catalyst with no difficulty due to its generality. The detailed reaction network, however, can be very complicated. Kumar et al.[23] proposed a detailed kinetic model which included more than 300 elementary steps, whereas the formation of aromatic species was ignored. Due to the big supercage of SAPO-34 catalyst, more condensed active intermediates may appear in the reaction process, which makes the detailed modeling work more difficult. Therefore, simplifications must be made to reduce the number of reaction steps. Froment[37] reconciled the oxonium methyl ylide mechanism and the hydrocarbon pool mechanism, and proposed a general scheme for MTO reaction and the corresponding coke formation over SAPO-34 catalyst. In the general reaction scheme, the active sites on the catalyst are divided into two types: acid sites on the catalyst surface, where carbenium ions are generated, and acid sites on the "coked" surface, where methylation, oligomerization, and β-scission occur. The deactivation of MTO process is assumed to follow the transformation of olefinic species to heavier species, which causes site coverage and pore blockage.
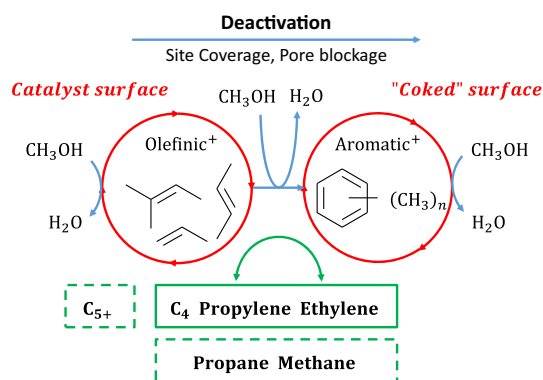
Figure 2. Simplified reaction scheme based on the dual-cycle mechanism.

[Color figure can be viewed at wileyonlinelibrary.com]

Inspired by the reconciled reaction scheme, reactions related to the dual-cycle mechanism could also be divided into two types, assuming the olefins-based cycle to occur on the acid sites of the catalyst surface, while the aromatics-based cycle occurring on the acid sites of the "coked" surface. The transformation of acid sites on the catalyst surface to acid sites on the "coked" surface is also considered, and the deactivation is a natural result of this process, which will be discussed later. The resulting reaction scheme is shown in Figure 2.

According to the dual-cycle mechanism, ethylene is usually supposed to be formed mainly *via* the aromatics-based cycle, and higher olefins are formed mainly *via* the olefins-based cycle. Alkanes are formed during the formation of olefin species, or transformation of olefin species to aromatic species, or aromatic species to more condensed species. However, the detailed mechanism of these transformations is still not clear and the reaction network would be too complicated to consider all these mechanisms. In the detailed kinetic model, Kumar et al.[23] assumed the aromatic species to be an inherent catalyst property, which resembles active sites. Therefore, a similar assumption could be made that both the olefinic and aromatic species are intrinsic properties of the catalyst. The detailed active intermediate species in both olefins-based and aromatics-based cycles are not distinguished, and only the amount of active sites occupied by these species, as well as their autocatalytic characteristic, is considered in the kinetic model. The active sites of the catalyst are denoted by *S*, which includes the protonated olefinic species and the free acid sites on the catalyst, and the protonated aromatics, are denoted by *R*. *S* and *R* are quantified as mass fraction per mass unit of catalyst, denoted by Y_S (dimensionless) and Y_R (dimensionless), respectively.

Under aforementioned assumptions, ethylene, propylene, and C4 species are treated as directly produced from methanol with the participation of *S* and *R*, and the higher olefins, which are given as a lumped species C5+, are produced only from *S*. The transformation of olefins-based cycle to aromatics-based cycle is assumed to occur with the participation of methanol and olefins. Alkanes including methane and propane are assumed to be produced *via* a similar routine as light olefins. Besides the main reactions, other side reactions could also be added to the model, as methylation, oligomerization, and β-scission reactions may also exist.

Meantime, the proposed reaction scheme should represent the main characteristics of the MTO reaction. As shown in Figure 2, three categories of reactions are considered: olefins-based cycle, aromatics-based cycle, and reactions involving the evolution of olefins-based cycle to aromatics-based cycle. In the current kinetic scheme, the autocatalytic reactions are implicitly taken into account by assuming each cycle to be a virtual lump of reaction species. The relative ratio of both cycles has significant influence on methanol conversion and product distribution. The detailed reaction network will be given in the "Reaction network" section.

Deactivation model

Researchers suggested that the deactivation of MTO process over SAPO-34 is caused by a gradual transformation of active intermediate species to less active polycyclic aromatics with time on stream.[38-42] Thus, the modeling of the time-dependent deactivation process should take the evolution of active species, deactivating species, and free acid sites of catalyst into consideration. Furthermore, the deactivating species may not only cover active sites, but also cause pore blockage, thus making the deactivation process more complex.

Wragg et al.[34] developed a simplified model to describe the induction period and deactivation of MTO process. In their model, Wragg et al. assumed that all aromatic and coke species in SAPO-34 catalyst are presented in protonated form, and thus the total number of Brønsted sites of the catalyst equals the number of free Brønsted sites and the number of Brønsted sites where the proton is residing on the adjacent aromatic and coke. Therefore, the deactivation process is caused by the transformation of active species to coke species, which reduces the available active sites. With their model, the experimental observations could be reproduced by the simulation data. However, the model is only descriptive, and gives very few information about the overall deactivation process.

In industrial applications, coke content is usually correlated to the deactivation process. Due to the narrow pore openings of SAPO-34 catalyst, aromatics could be too bulky to diffuse out of the catalyst, and thus trapped inside the catalyst and finally grew into coke. Therefore, the coke content determined *via* the offline method contains both active and inactive aromatic species. In the current work, the active aromatic intermediates and coke species are not distinguished for simplicity, and a separate model is proposed afterwards to account for the difference between the active aromatic species and coke. By assuming that all aromatic species are present in protonated form, the sum of Y_S and Y_R should be constant, and is an intrinsic characteristic for the catalyst. When catalyst is fully deactivated, all active sites are assumed to be occupied by coke species, then a maximum coke content, c_c^{max}, could be obtained. Therefore, the quantities of *S* could be expressed as

$$Y_S = c_c^{max} - Y_R = c_c^{max} - c_c \qquad (1)$$

where c_c (dimensionless, mass unit of coke per mass unit of catalyst) is the coke content; c_c^{max} represents the maximum capacity of catalyst to deposit coke under given operation conditions. Note that the value of c_c is critical in the current model, and it can be directly measured.

Although deactivating species in MTO process are still ambiguous, it is generally considered that different intermediate species show different activities. Ying et al.[43] suggested that under high temperatures, methylbenzenes and methylnaphthalenes could be regarded as active species, while heavier species are inactive. They also found that phenanthrene and pyrene are undetectable at initial time on stream. Therefore, it is reasonable to assume that all the coke
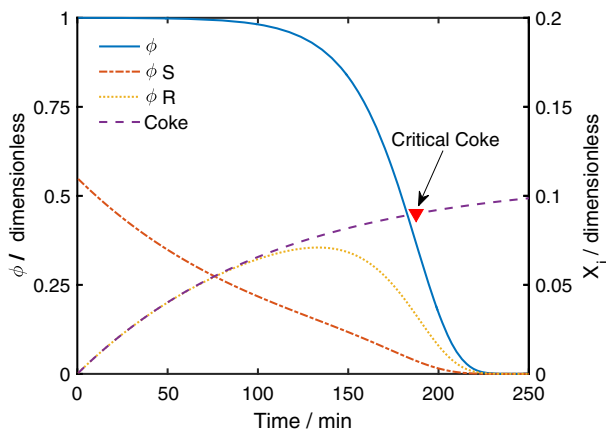
Figure 3. A schematic simulation for the evolution of ϕ (left axis), ϕS (right axis), ϕR (right axis), and coke (right axis) with time on stream.

The critical coke content used in the simulation is 0.09, which is marked in the figure. [Color figure can be viewed at wileyonlinelibrary.com]

deposition at initial time on stream are active, and the deactivating species are formed after a certain time on stream. With this assumption, evolution of active sites with time on stream could be shown in Figure 3, where ϕS represents the active olefins-based species and ϕR represents the active aromatics-based species.

Figure 3 clearly shows that, at initial time on stream, the amount of active aromatic species is equivalent to coke; then prior to the beginning of the deactivation process, the difference between active aromatic species and coke becomes quite significant. As marked in the figure, the critical coke content is a key parameter, since it determines when the decline of active aromatic species becomes significant, thus reflecting the efficiency of catalyst. A large critical coke content suggests that most coke species deposited on the catalyst is active. A deactivation model that could reproduce all these features is proposed to account for the catalyst activity changes, as shown in the following

$$\frac{d\phi}{dc_c} = -k_a \phi \left(\frac{c_c^{max} - c_c}{c_c^{max} - c_c^{cri}} \right)^{-n}. \quad (2)$$

Integrate Eq. 2 and the following equation is obtained:

$$\phi = \left\{ \frac{\exp\left[-\left(\frac{c_c^{max} - c_c^{cri}}{c_c^{max} - c_c} \right)^{n-1} \right]}{\exp\left[-\left(\frac{c_c^{max} - c_c^{cri}}{c_c^{max}} \right)^{n-1} \right]} \right\}^m \quad (3)$$

where

$$m = \frac{k_a}{n-1} \cdot \left(c_c^{max} - c_c^{cri} \right). \quad (4)$$

In Eq. 3, c_c^{max} denotes the maximum coke content, which theoretically corresponds to the extreme case where the methanol conversion drops to zero; c_c^{cri} is the critical coke content; the value of n is related to the experimental data, and could reflect the significant decrease of ϕR when the coke content c_c approaches c_c^{cri}; m is a constant, which should be chosen according to the deactivation properties.

Note that even if catalyst is fully deactivated, not all aromatic species are transformed into inactive species. However,

these active species may be inaccessible due to the hindered diffusion by the confined coke species, which might be represented in the deactivation model.

Experimental

### Catalyst and experimental procedure

Industrial DMTO catalyst obtained from Chia Tai Energy Materials was used for kinetic study. Its typical properties have been described in the literature[1]: the BET surface area is greater than $180 \text{ m}^2 \text{ g}^{-1}$, the pore volume greater than $0.15 \text{ cm}^3 \text{ g}^{-1}$, and the particle density around 1.5–1.8 g cm^{-3}. The DMTO catalyst is typical Type A particles according to Geldart particle classification,[44] which has excellent fluidization performance. Due to commercial confidentiality, the detailed characterization of the DMTO catalyst could not be given in open literature.

The kinetic study was performed in a laboratory scale fluidized bed reactor. The diagram of the reaction equipment could be found in a previous work.[45] The reactor has an internal diameter of 0.19 m, and a total length of 0.33 m. Two filters were used in series at the outlet of the reactor for solid–gas separation. Experiments with different weight hourly space velocity (WHSV) were carried out by altering catalyst loading while keeping inlet feed rate constant. For kinetic studies, the amount of catalyst loaded was in the range of 2–5 g, while experiments with less catalysts were also conducted to investigate the activity change with time on stream, where 1 g, 0.5 g, and 0.25 g catalyst were used, respectively. The aqueous or pure methanol was fed with a piston pump to a vaporizer placed before the reactor to guarantee good vaporization. The amount of water fed to the reactor is represented with the water/methanol mass ratio, X_{w0}. According to the operation conditions, a total amount of 10.5 g h^{-1} aqueous methanol, with 80 wt % methanol (denoted by $X_{w0} = 0.25$), or a total amount of 8.4 g h^{-1} pure methanol (denoted by $X_{w0} = 0$) was fed. Nitrogen was added to keep the gaseous flow stable, with a flow rate of 80 mL min^{-1}. The feedstock and corresponding catalyst load were chosen so that the fluidized bed was operated under the bubbling fluidization region, which guarantees good gas–solid contact efficiency. The experiments under different superficial velocities are carried out to study the effect of transport limitations and it is found that gas superficial velocity of 3.4 cm s^{-1} used in most of the experiments in this work could possess negligible transport limitations. Before feeding aqueous or pure methanol, the reactor was heated to 500°C with nitrogen atmosphere and kept for 60 min at that temperature. Then the reactor was set to the desired temperature. On-line analysis of reaction products were performed with Agilent 7890A gas chromatograph equipped with FID detector and PoraPLOT Q-HT capillary column (25 m × 0.53 mm × 0.02 mm). Coked catalyst was sampled at different time on stream to determine coke content by thermogravimetric analysis.

Experimental results

The evolution of methanol conversion, product selectivity, and coke content with time on stream obtained in the fluidized bed reactor is shown in Figure 4. It is observed that methanol conversion increases slightly from 97.5% to more than 99.0% at the initial 5 min (Figure 4A), indicating that even at a rather high temperature, methanol conversion over SAPO-34 catalyst has an induction period. During this period, the formation of hydrocarbon pool species can increase catalyst activity, which
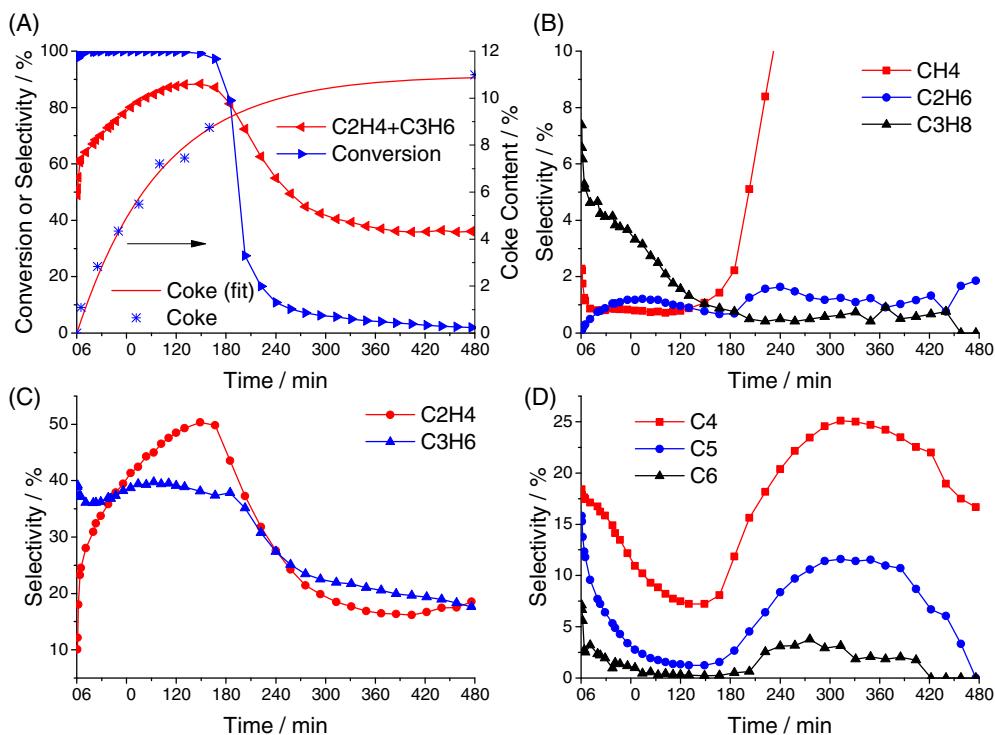
Figure 4. Evolution of conversion, product selectivity, and coke content with time on stream in a fluidized bed reactor. Temperature: 450°C; WHSV = 1.68 $g_{MeOH} \cdot g_{cat}^{-1} \cdot h^{-1}$; X_{w0} = 0.25 (g of water) (g of methanol)$^{-1}$.

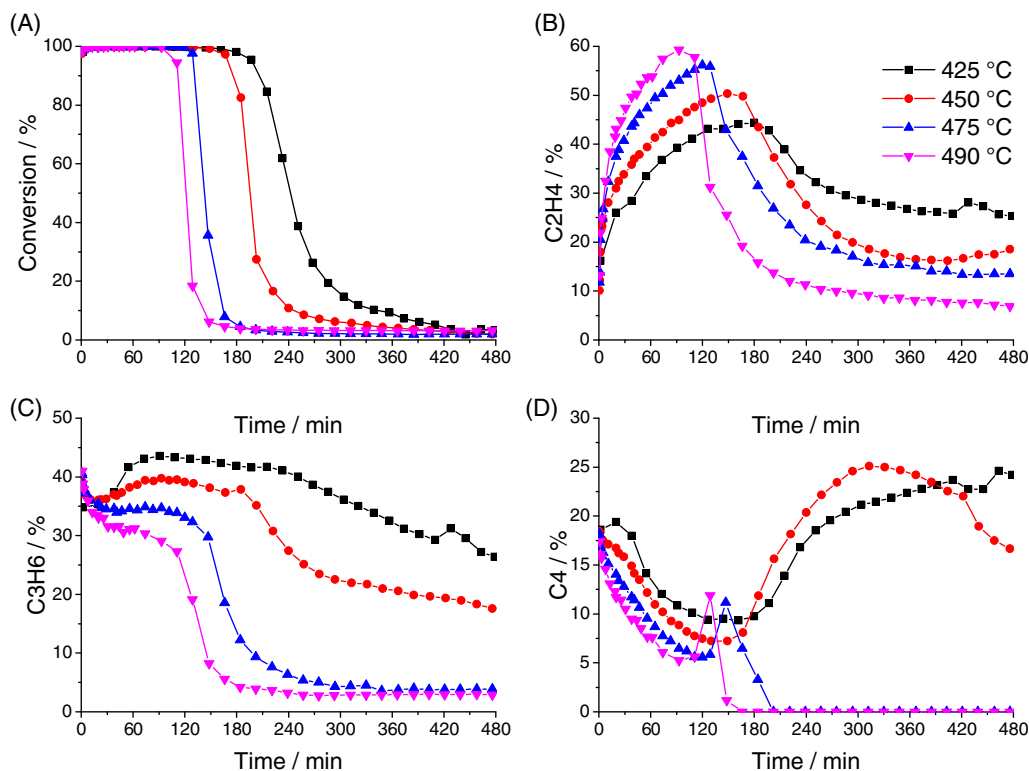[Color figure can be viewed at wileyonlinelibrary.com]

is evidenced by the relatively high selectivity to methane and propane (see Figure 4B). Selectivity to olefins also changes dramatically. For instance, selectivity to ethylene increases from about 10 wt % to 28 wt %, and selectivity to propylene decreases from 40 wt % to 35 wt % (see Figure 4C). Dai et al.[17] suggested that aromatics-based cycle is formed *via* olefins-based cycle during early stages of MTO reaction, and for olefins-based cycle, propylene and C_4 to C_6 olefins are the main products. These conclusions could explain the increase of selectivity to ethylene and decrease of propylene and C_4 to C_6 olefins at initial time, as shown in Figure 4C, D. However, the induction period is quite short due to the relatively high temperature in our experiments.

As MTO reaction evolves into steady-state operation, aromatics-based cycle dominates the reaction. Selectivity to ethylene keeps increasing, while propylene selectivity increases slightly to a maximum and then decreases. Selectivity to C_4–C_6 decreases constantly with time on stream. Hereijgers et al.[41] suggested that increase of selectivity to light olefins and decrease of selectivity to high olefins (C_4 to C_6) with time on stream could be attributed to product shape selectivity of catalyst. However, the change from olefins-based cycle to aromatic cycle in MTO reaction can also explain these phenomena. Other reactions also contribute to the total product distribution. Tian et al.[1] found that for catalyst with weak acidity, alkene methylation and cracking are efficient and selective routes for olefin production. They suggested that methylation reaction exists in the whole MTO process, though hindered by high-methanol conversion. The methylation reaction may be the underlying reason for the relatively complex kinetic behavior of propylene and C_4. A careful check with Figure 4C, D shows that the decrease of propylene with time on stream occurs before the abrupt decrease of methanol conversion, while the decreasing of C_4 and high olefins starts to slow

down at that point. The results might be caused by the consecutive methylation of propylene to higher olefins. Since catalyst may lose part of its activity before the abrupt transition of methanol conversion, methylation reaction might be enhanced at this stage. Therefore, methylation reaction should be included in the MTO reaction network. During steady-state operation, selectivity to methane remains at a low level and starts to increase only before the abrupt transition of methanol conversion. Meanwhile, selectivity to propane keeps decreasing with time on stream, though the decreasing rate is quite low, which indicates that propane might be formed along with the conversion of aromatics to more active species.

After the catalyst deactivates, as can be seen from Figure 4D, the selectivities to C_4 and high olefins increase with time on stream, while the selectivities to ethylene and propylene decrease rapidly. One possible explanation is that it is due to the enhanced methylation of light olefins with unconverted methanol in the reactor. As shown in the figure, the decreasing of ethylene is much faster than that of propylene, which indicates that the methylation of ethylene to propylene might also exist. Selectivity to methane starts to increase before the abrupt deactivation, which indicates that formation of methane could be closely related to catalyst deactivation. Schulz et al.[46] suggested that methane may come from the growth and dehydrogenation of coke species. The results could be used to explain the current observations. Selectivity to propane decreases rapidly when catalyst is not deactivated, and gradually approaches to zero after deactivation. Figure 4A also shows the evolution of coke content with time on stream. The rate of coke deposition is quite high initially and becomes slower with time on stream.

The results in Figure 4 suggest that both olefins-based and aromatics-based cycles are important in the MTO reaction over SAPO-34 catalyst. At initial stage, olefins-based cycle

Figure 5. Effect of temperature on conversion of methanol (A) and selectivity to ethylene (B), propylene (C), butylene (D) with time on stream. WHSV $= 1.68$ $g_{MeOH} \cdot g_{cat}^{-1} \cdot h^{-1}$; $X_{w0} = 0.25$ (g of water) (g of methanol)$^{-1}$.

[Color figure can be viewed at wileyonlinelibrary.com]

dominates the reaction, and the formation rate of aromatics is high. As aromatics-based cycle is more active than that of olefins-based cycle, methanol conversion is enhanced with the formation of aromatics-based cycle. The current model could well capture the initial increase of methanol conversion. At the steady stage, highly active aromatics act as main hydrocarbon pool species, and the conversion is so fast that almost no excess methanol remains in the reactor. The evolution of selectivity to main products during this stage can be closely related to the evolution of olefins-based and aromatics-based cycles. When catalyst starts to deactivate, active hydrocarbon species are transformed into inactive heavy species, and methane can be generated simultaneously. Furthermore, since active and inactive coke are not distinguished in the current model, a separate phenomenological deactivation model in given (Eq. 2 and 3) to account for the difference between coke and active species, and thus the deactivation process of the MTO reaction could be depicted.

Effect of operation conditions

Effect of Temperature. Figure 5 shows the effect of temperature on the evolution of product selectivity with time on stream. As can be seen, catalyst lifetime becomes shorter when temperature increases from 425°C to 490°C. The coke content determined prior to the abrupt decrease of methanol conversion under different temperatures is quite close, which suggests that the shorter catalyst lifetime under high temperatures is caused by a higher coke formation rate. The results also show that, as temperature increases from 425°C to 490°C, selectivity to ethylene increases, while selectivity to propylene and C$_4$ decreases. Ying et al.[28] explained these observations as enhanced olefin cracking reactions at higher temperatures. Wu et al.[47] also found that

temperature is the decisive factor for ethylene/propylene ratio, and high temperature favors ethylene production. This finding is in accordance with our experimental results. The increase of selectivity to C$_4$ might be attributed to methylation reactions over partially deactivated catalyst. Under higher temperatures, the deactivation of catalyst becomes more rapid, thus the increase of higher olefins is not pronounced.

Effect of WHSV. Figure 6 shows the effect of WHSV on methanol conversion and olefin selectivity. With higher WHSV, catalyst lifetime is shorter as the amount of methanol fed to the catalysts is increased. When methanol conversion is shown as the function of cumulative amount of methanol fed to catalyst, as shown in Figure 7, the results show that methanol conversion starts to decrease only after about 5–6 g methanol is fed to 1 g catalyst. Methanol conversion shows a similar trend of initially increasing, then almost keeping constant, and finally decreasing for all the experiments. Considering the autocatalytic characteristic of methanol conversion, the initial increase of catalyst activity is quite natural. As the active intermediate species evolve to heavier deactivating species, catalyst may lose some activity. When the formation and consumption of active intermediate species are comparable, catalyst activity may keep constant, resulting in an almost constant methanol conversion. When catalyst deactivates, methanol conversion decreases significantly. Figure 7 also shows that, under rather high WHSV, where methanol conversion is less than 90%, the evolution of methanol conversion is also similar. The result suggests that catalyst activity might not follow a gradual decrease with coke deposition.

From Figures 6 and 7, it could be found that the evolution of methanol conversion after deactivation is quite different for different WHSVs. Chen et al.[48] suggested that coke deposition
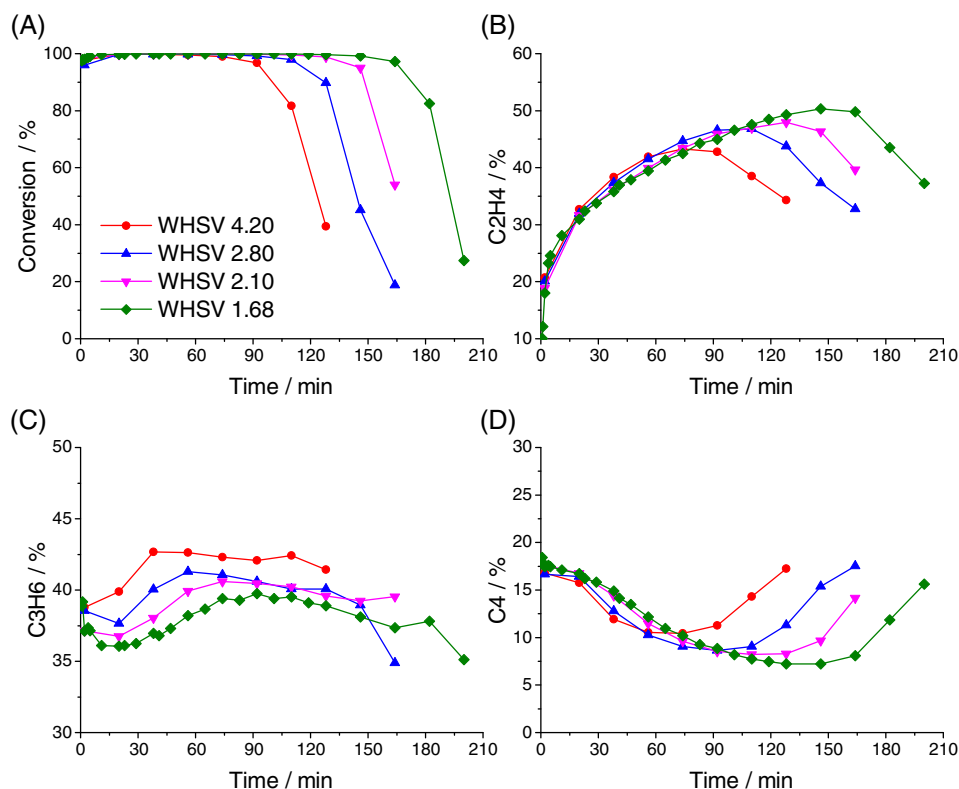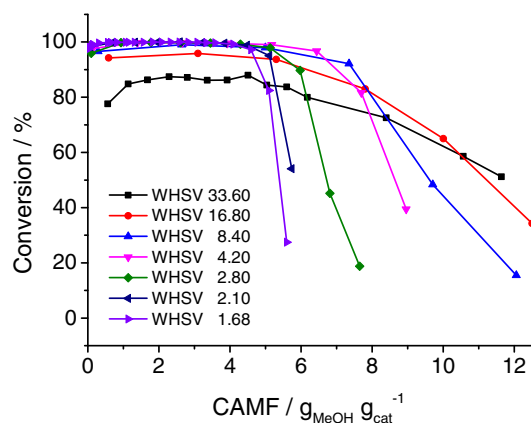
Figure 6. Effect of WHSV on conversion of methanol (A) and selectivity to ethylene (B), propylene (C), butylene (D) with time on stream. Unit for WHSV: $g_{MeOH} \cdot g_{cat}^{-1} \cdot h^{-1}$. Temperature: $450 °C$; $X_{w0} = 0.25$ (g of water) (g of methanol)$^{-1}$.

on SAPO-34 catalyst depends on the cumulative amount of methanol fed to the catalysts as well as the conversion of oxygenates. They concluded that a lower WHSV can result in a higher conversion of oxygenates and meantime a higher coke formation rate. Determination of coke content prior to the abrupt change of methanol conversion shows that a higher WHSV results in a lower coke content. The experimental results could also be explained as a lower WHSV causing a severer deactivation, which suggests that the coke species under different WHSVs might be different. Figure 6 also shows that the maximum selectivity to ethylene and propylene varies under different WHSV, which could be attributed to the different coke deposition behavior.

In the current work, a separate deactivation model is used to represent the deactivation process, as shown in Eq. 2. The above-mentioned results suggest that the coking behavior is different for different WHSVs and needs further attention. Therefore, an empirical correlation is proposed in the current work to calculate c_c^{cri} under various WHSVs, which would be discussed in the Kinetic Parameters.

Effect of Water. The effect of water on methanol conversion and olefin selectivity is shown in Figure 8. In the experiments, nitrogen is added to keep methanol partial pressure and inlet gas velocity the same. Catalyst lifetime is prolonged with higher water fraction in the reactant, due to the dilution of methanol and attenuation of all the reactions.[25,49] The competition of water with methanol and olefins for access to the acid sites could also contribute to the prolonging of catalyst lifetime,[50] which may be explained as increased catalyst efficiency with higher water content. Shahda et al.[51] found that selectivity to light olefins increases when the fraction of water

is increased in their experiments. De Wispelaere et al.[52] also reported water could help lower the free energy barrier during olefin formation process. However, we found that the variation of product selectivity for different water fractions is negligible in the current work. This might be caused by the relatively large amount of water that exists in the reaction system during the MTO process, since in theory more than half of methanol will be transformed to water, which is much larger than the amount of water added to dilute the feed.

Figure 7. Effect of WHSV on methanol conversion with cumulative amount of methanol fed to the catalysts. Unit for WHSV: $g_{MeOH} \cdot g_{cat}^{-1} \cdot h^{-1}$. Temperature: $450 °C$; $X_{w0} = 0.25$ (g of water) (g of methanol)$^{-1}$.
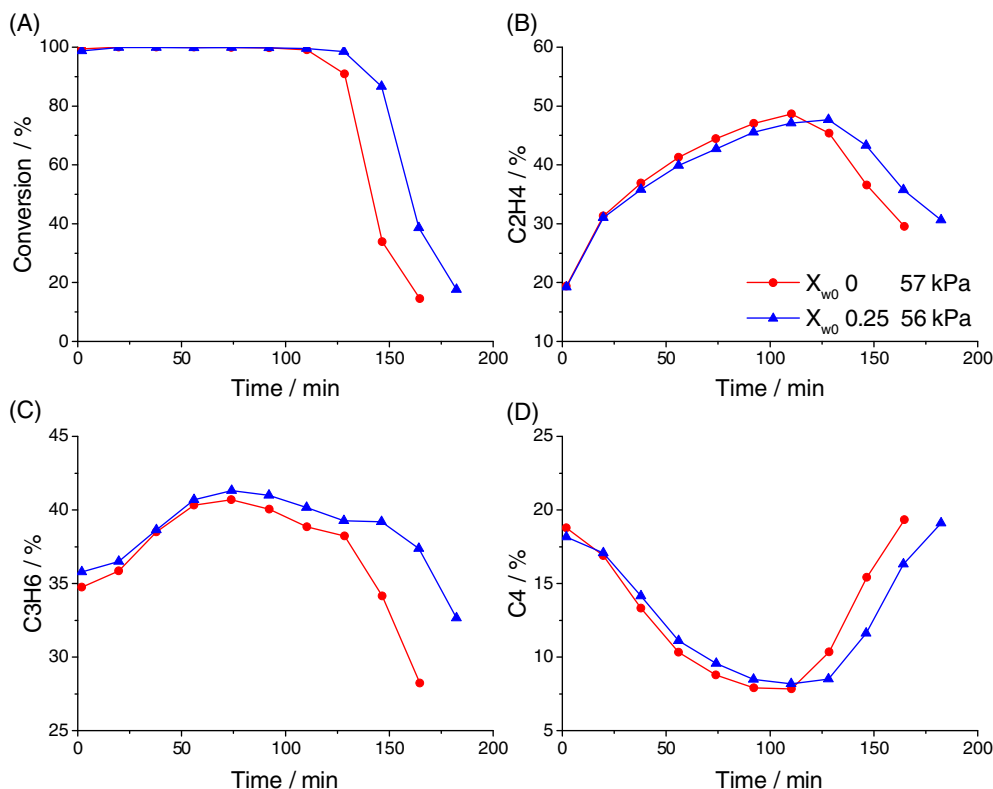
Figure 8. Effect of water on conversion of methanol (A) and selectivity to ethylene (B), propylene (C), C_4 (D) with time on stream. Temperature: $450\,^{\circ}$C; WHSV $= 2.10\ g_{MeOH}\cdot g_{cat}^{-1}\cdot h^{-1}$; For $X_{w0} = 0.25$ (g of water) (g of methanol)$^{-1}$, $N_2 = 37\ ml\cdot min^{-1}$, while for $X_{w0} = 0$ (g of water) (g of methanol)$^{-1}$, $N_2 = 80\ ml\cdot min^{-1}$.

[Color figure can be viewed at wileyonlinelibrary.com]

In the literature, the effect of water is usually considered by an empirical expression[25-28]:

$$\theta_{w} = \frac{1}{1 + K_{w}X_{w}} \tag{5}$$

where K_{w} is kinetic parameter and X_{w} is the water mass fraction in the reaction medium, which is either calculated *via* empirical correlations or obtained from the experiments in presence of water. In the current work, it is found that with higher water content, the critical coke content should be larger to simulate the deactivation process, which suggests a more efficient use of the catalyst. Since the variation of water content is quite small in the current work, the change of critical coke content is negligible, and it is assumed that the critical coke content is identical for different water contents.

Modeling

Methodology for the kinetic study

Ideally mixed flow has been assumed in the laboratory fluidized bed reactor, given that the scale of the reactor is rather small. The concentration of species in the reactor is the same with the outlet flow, so the following continuity equation is obtained:

$$\frac{d\rho_{j}}{dt} = k_{f}\left(\rho_{j}^{in} - \rho_{j}\right) + R_{j} \tag{6}$$

where ρ_{j}^{in} and ρ_{j} represent the inlet and outlet mass concentration of species j, respectively, which are calculated on the basis of gas-phase volume, k_{f} represents the ratio of volume flow rate of the feed to gas-phase volume (min^{-1}), t is the time on stream

(min), and R_{j} is the reaction rate of species (j(kg $\cdot$ m^{-3} $\cdot$ min^{-1}). The MTO reaction is a volume expansion reaction as 1 mol methanol will become 1 mol water and some other products. Due to the addition of nitrogen as diluent in the reaction, our preliminary simulations show that the volume expansion does not make the results notably different, thus the effect of volume expansion has been neglected in the simulations.

The kinetic parameters have been estimated by a hybrid genetic algorithm in combination with the steepest descent method. Optimization of the kinetic parameters was performed by minimizing the error objective function, which is the difference between the experimental and calculated values of the weight fractions of the MTO products:

$$EOF = \frac{\sum\limits_{n_{l}}^{i=1}\sum\limits_{n_{exp}}^{j=1}\left(X_{i,j} - X_{i(cal),j}\right)^{2}}{n_{l}n_{exp}} \tag{7}$$

where, $X_{i,\ j}$ and $X_{i(cal),\ j}$ are the experimental and calculated values of weight fraction of lump i on a water free basis at the experimental point j.

The expression of the rate constant in Arrhenius equation is in the form of reference temperature (723 K):

$$k_{i} = k_{0i}\exp\left[-\frac{Ea_{i}}{R}\left(\frac{1}{T} - \frac{1}{723}\right)\right] \tag{8}$$

In Eq. 8, k_{i} is the reaction rate constant of reaction i, k_{0i} is the rate coefficient of reaction i at the reference temperature (723 K), Ea_{i} is the activation energy of reaction i, R is the molar gas constant (kJ $\cdot$ mol^{-1} $\cdot$ K^{-1}), and T is the reaction temperature (K).

Table 1. Reaction Network and Rate Equation of MTO Process

Category	Reaction	Rate Equation
Olefins-based cycle	$MeOH \xrightarrow{S} CH_4 + H_2O$	$r_1 = k_1 \rho_{MeOH} Y_S \phi$
	$MeOH \xrightarrow{S} C_2H_4 + H_2O$	$r_2 = k_2 \rho_{MeOH} Y_S \phi$
	$MeOH \xrightarrow{S} C_3H_6 + H_2O$	$r_3 = k_3 \rho_{MeOH} Y_S \phi$
	$MeOH \xrightarrow{S} C_3H_8 + H_2O$	$r_4 = k_4 \rho_{MeOH} Y_S \phi$
	$MeOH \xrightarrow{S} C_4H_8 + H_2O$	$r_5 = k_5 \rho_{MeOH} Y_S \phi$
	$MeOH \xrightarrow{S} C_{5+} + H_2O$	$r_6 = k_6 \rho_{MeOH} Y_S \phi$
	$MeOH + C_2H_4 \xrightarrow{S} C_3H_6 + H_2O$	$r_7 = k_7 \rho_{MeOH} \rho_{C2H4} Y_S \phi$
Transformation of olefins-based cycle to aromatics-based cycle	$MeOH + S \rightarrow R + H_2O$	$r_8 = k_8 \rho_{MeOH}^{0.3} Y_S$
	$C_2H_4 + S \rightarrow R$	$r_9 = k_9 \rho_{C2H4}^{0.3} Y_S$
	$C_3H_6 + S \rightarrow R$	$r_{10} = k_{10} \rho_{C3H6}^{0.3} Y_S$
	$C_4H_8 + S \rightarrow R$	$r_{11} = k_{11} \rho_{C4H8}^{0.3} Y_S$
	$C_{5+} + S \rightarrow R$	$r_{12} = k_{12} \rho_{C_{5+}}^{0.3} Y_S$
Aromatics-based cycle	$MeOH \xrightarrow{R} CH_4 + H_2O$	$r_{13} = k_{13} \rho_{MeOH} Y_R \phi$
	$MeOH \xrightarrow{R} C_2H_4 + H_2O$	$r_{14} = k_{14} \rho_{MeOH} Y_R \phi$
	$MeOH \xrightarrow{R} C_3H_6 + H_2O$	$r_{15} = k_{15} \rho_{MeOH} Y_R \phi$
	$MeOH \xrightarrow{R} C_3H_8 + H_2O$	$r_{16} = k_{16} \rho_{MeOH} Y_R \phi$
	$MeOH \xrightarrow{R} C_4H_8 + H_2O$	$r_{17} = k_{17} \rho_{MeOH} Y_R \phi$

Reaction network

Based on the reaction scheme proposed in the Reaction Kinetics, the reaction network and rate equations are shown in Table 1. Note that a large variety of reactions, such as methylation, oligomerization, and cracking reactions are considered in the reaction network initially, and most of them are removed during the parameter estimation due to the large uncertainty of these reactions. For the olefins-based and aromatics-based cycle, all the parallel reactions are assumed to be first order in methanol, and the methylation of ethylene is assumed to be first order in methanol and ethylene. The transformation of olefins-based cycle to aromatics-based cycle is very complicated, and the details of this process are far from known. According to recent mechanism studies regarding to MTO process,[42] the actual transformation may involve many different intermediate species with different reaction orders. In this work, it is assumed that the transformation occurs directly with the participation of methanol and some main reaction products, which represents a significant simplification. A reaction order of 0.3 is obtained by best fitting the experimental data. As the true reaction network and reaction orders are hard to determine, the reaction order of 0.3 might represent the gross influences of all elementary reactions in the transformation of olefins-based cycle to aromatics-based cycle. Despite its empirical nature, the reaction order of 0.3 may indicate that the corresponding reactions are less sensitive to the concentration of methanol and olefins than other reactions. The methanol conversion and product formation rates are written as Eq. 9–17, where ρ_s is the density of the catalyst bed, which is calculated on the basis of gas-phase volume, and ϕ is the deactivation function (see Eq. 3). Note that in Eq. 9–17, the fractional stoichiometric coefficients are obtained based on the mass balance. For example, for the reaction $MeOH + C_2H_4 \rightarrow C_3H_6 + H_2O$, where 1 mol of methanol and 1 mol of ethylene are converted to 1 mol of propylene and 1 mol of water, the mass balance is established by considering $\frac{32}{32+28}$ mass unit of methanol and $\frac{28}{32+28}$ mass unit of ethylene transfer to $\frac{42}{18+42}$ mass unit of propylene and $\frac{18}{18+42}$ mass unit of water.

$$R_{MeOH} = -\left(\sum_{i=1}^{6} r_i + \frac{8}{15} r_7 + r_8 + \sum_{i=13}^{17} r_i \right) \cdot \rho_s \quad (9)$$

$$R_R = \frac{14}{32} r_8 + r_9 + r_{10} + r_{11} + r_{12} \quad (10)$$

$$R_{CH_4} = \frac{14}{32} (r_1 + r_{13}) \cdot \rho_s \quad (11)$$

$$R_{C_2H_4} = \left[\frac{14}{32} (r_2 + r_{14}) - \left(\frac{7}{15} r_7 + r_9 \right) \right] \cdot \rho_s \quad (12)$$

$$R_{C_3H_6} = \left[\frac{14}{32} (r_3 + r_{15}) + \frac{7}{10} r_7 - r_{10} \right] \cdot \rho_s \quad (13)$$

$$R_{C_3H_8} = \frac{14}{32} (r_4 + r_{16}) \cdot \rho_s \quad (14)$$

$$R_{C_4} = \left[\frac{14}{32} (r_5 + r_{17}) - r_{11} \right] \cdot \rho_s \quad (15)$$

$$R_{C_{5+}} = \left(\frac{14}{32} r_6 - r_{12} \right) \cdot \rho_s \quad (16)$$

$$R_{H_2O} = \frac{18}{32} \left(\sum_{i=1}^{6} r_i + \frac{8}{15} r_7 + r_8 + \sum_{i=13}^{17} r_i \right) \cdot \rho_s \quad (17)$$

Kinetic parameters

The parameters are estimated with experimental data from a laboratory scale fluidized bed reactor. Considering the deactivation correlation proposed in Eq. 3, we assume that the deactivation has no influence on the reaction prior to the abrupt change of the methanol conversion. Therefore, the parameters are estimated with experimental data prior to the abrupt deactivation. Then Eq. 3 is used to account for the deactivation process. The corresponding objective function EOF is calculated to be 3.7×10^{-3}. The estimated kinetic parameters and the 95% confidence interval are listed in Table 2.

To apply Eq. 3 to the kinetic model, the maximum coke content, c_c^{max}, and critical coke content, c_c^{cri}, should be determined. Theoretically, both the maximum and critical coke content should be related to the intrinsic properties of catalyst, such as micropore volume. However, in this work, we only use the industrial catalyst for DMTO process, and it is hard to obtain such relation with only one type of catalyst. Therefore, the effect of intrinsic catalyst properties on the maximum and critical coke content is not considered. Rather than that, we focus on the influence of operating conditions on the critical

Table 2. Kinetic Parameters

Kinetic Constant	k_{i0}*	Ea_i†
k_1	0.81 ± 0.085	-0.040 ± 0.0030
k_2	10.44 ± 0.44	0.84 ± 0.061
k_3	13.94 ± 0.59	1.19 ± 0.098
k_4	1.94 ± 0.11	-0.78 ± 0.071
k_5	6.98 ± 0.32	0.82 ± 0.062
k_6	6.01 ± 0.28	-1.11 ± 0.081
k_7	22.98 ± 1.6	1.80 ± 0.17
k_8	0.017 ± 0.0011	-1.47 ± 0.14
k_9	0.0074 ± 0.00048	35.02 ± 1.5
k_{10}	0.012 ± 0.00084	35.05 ± 1.0
k_{11}	0.0044 ± 0.00026	35.03 ± 2.5
k_{12}	0.0044 ± 0.00029	35.06 ± 2.0
k_{13}	0.65 ± 0.048	-10.13 ± 0.92
k_{14}	49.95 ± 3.9	28.79 ± 0.56
k_{15}	34.03 ± 2.6	-18.38 ± 0.56
k_{16}	1.15 ± 0.12	1.20 ± 0.075
k_{17}	6.39 ± 0.56	-18.39 ± 0.83

*First order: $m^3 \cdot kg^{-1} \cdot min^{-1}$; Second order: $(m^3 \cdot kg^{-1})^2 \cdot min^{-1}$.
†$kJmol^{-1}$.

coke content. The maximum coke content for $450°C$, $475°C$ and $490°C$ is determined to be 0.110, 0.117, and 0.122, respectively, where the experiments are performed with a WHSV of 1.68 $g_{MeOH} \cdot g_{cat}^{-1} \cdot h^{-1}$ for 8 h to make sure that the maximum coke content is obtained and the determined result is assumed to be the same for all the other operation conditions under the same temperature.

The value of c_c^{cri} is estimated with methanol conversion data under different WHSVs, which is shown in Figure 6A. According to the estimation results, the relationship between c_c^{cri} and WHSV $(g_{MeOH} \cdot g_{cat}^{-1} \cdot h^{-1})$ is correlated with Eq. 18. Different combinations of m and n are also tested, and the best fitting result is $m = 1$ and $n = 6$. We would stress that, however, it should be extrapolated to operation conditions other than the experiments with great caution. In fact, the hypothetical evolution of catalyst activity is considered in the proposed deactivation model, and the kinetic parameters are related to this hypothetical catalyst activity for simplicity. We understand that it may not reflect the reality, however, such hypothesis provides a simple yet useful way to obtain the kinetic parameters by fitting the experimental data in the current kinetic model.

$$c_c^{cri} = 0.10 - 0.02 \ln(\text{WHSV}). \qquad (18)$$

As discussed in the "Experimental" section, the relationship between WHSV and critical coke content is quite complicated. In the reactor models, the effect of WHSV is usually expressed as the effect of contact time, and its influence is correlated with reaction orders. In the current model, the reaction orders of the transformation of olefins-based cycle to aromatics-based cycle are quite important to reveal the effect of WHSV and reactant partial pressure on the reaction results. As the true reaction orders are unknown, some assumptions are made regarding to the reaction orders. For this reason, the effect of WHSV might not be fully represented with the current reactor model and the assumed reaction orders. Thus, the correlation shown in Eq. 18 is required to reproduce the experimental observations.

Considering that the current correlation is only an empirical relationship obtained with experiments of WHSV ranging from 1.68 to 4.20 $g_{MeOH} \cdot g_{cat}^{-1} \cdot h^{-1}$, further extending this correlation to a wider range of WHSV needs to be carefully

checked. According to our experimental observations, it seems to be more reasonable to use c_c^{cri} for the WHSV of 4.20 to represent the c_c^{cri} for WHSVs higher than 4.20, while use c_c^{cri} for the WHSV of 1.68 to calculate the c_c^{cri} for WHSVs lower than 1.68. The correlation is suitable for the simulation of the current experimental work, as well as the modeling of pilot and industrial MTO plants.

Model evaluation

With the proposed model, the major experimental observations could be well captured. Figures 9–11 show the comparison of the experimental and calculated mass fraction of each lump with time on stream. The lines represent the calculation results using the kinetic model and the points are the experimental results. The good agreement of the results for a wide
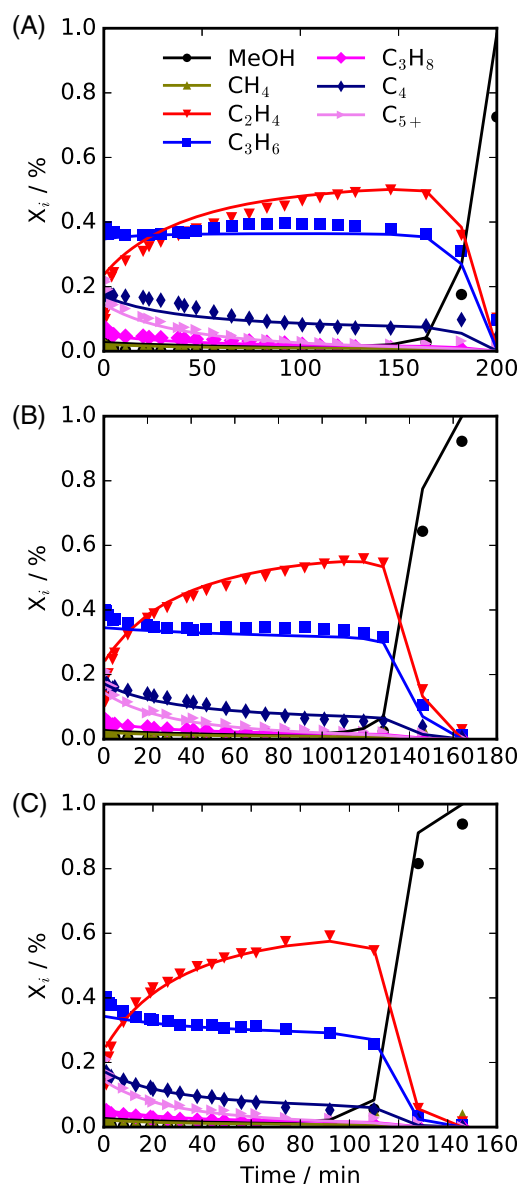
Figure 9. Comparison of the experimental and calculated mass fraction of each lump with time on stream: the effect of temperature, (A) 450°C, (B) 475°C, and (C) 490°C. Dots: Experiment; Lines: Calculation.

[Color figure can be viewed at wileyonlinelibrary.com]
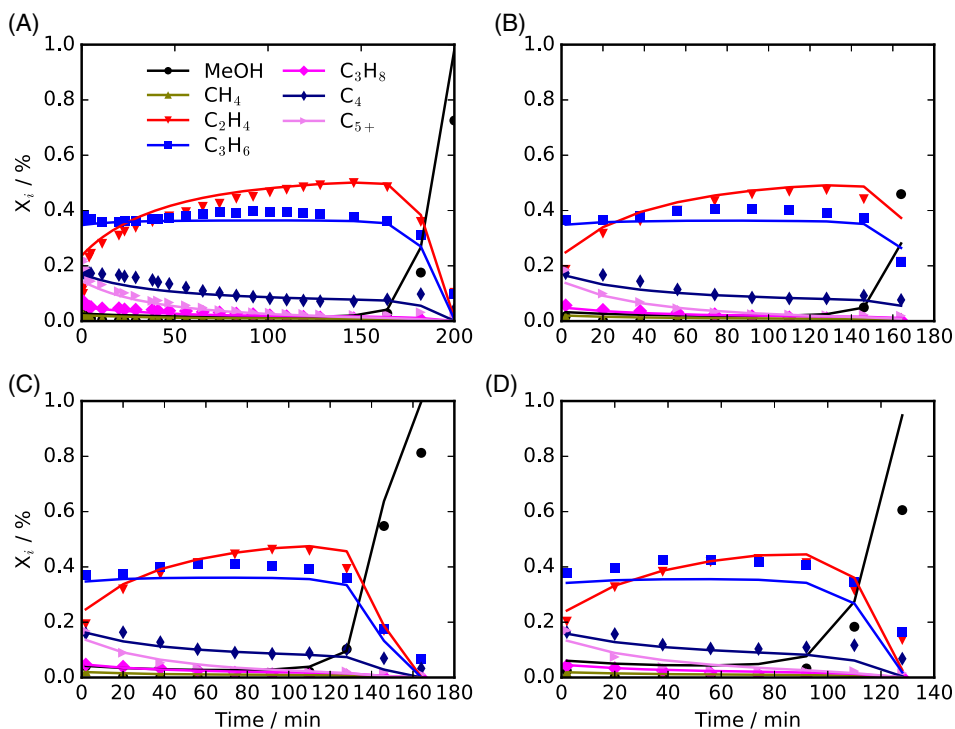
Figure 10. Comparison of the experimental and calculated mass fraction of each lump with time on stream: the effect of WHSV. WHSV ($g_{MeOH} \cdot g_{cat}^{-1} \cdot h^{-1}$): (A) 1.68, (B) 2.10, (C) 2.80, and (D) 4.20. Dots: Experiment; Lines: Calculation.
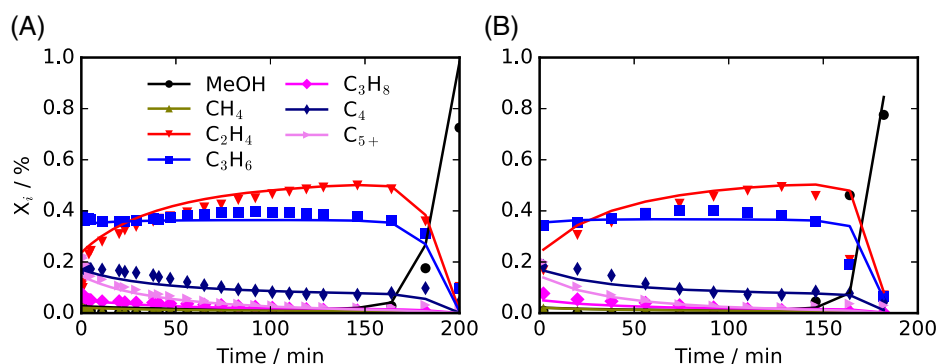
[Color figure can be viewed at wileyonlinelibrary.com]

range of operation conditions, namely temperature, WHSV, and water fraction in the feed, indicates that the current model provides a robust kinetic modeling approach for the MTO process.

Figure 9 depicts the influence of temperature on the MTO reaction. As can be seen, with elevated temperature, production of propylene and C_4 decreases, while production of ethylene increases. Note that the activation energies for olefin interconversions are relatively small (see Table 2), which indicates that temperature may have a minor influence on these reactions. Since the kinetic parameters are estimated from experimental data for major lumps, only the effect of temperature on the overall reaction results could be obtained. As shown in Table 2, some of the activation energies calculated are negative, which may suggest that the influence of temperature on these reactions is negative. In fact, although the current

model is based on the fundamental dual-cycle reaction mechanism, it does not consider all the elementary reactions and only apparent activation energies could be obtained. Some apparent activation energies appear to be negative because the reaction network is still highly simplified. The influence of diffusion and adsorption process may also be included in the kinetic parameters. Meanwhile, the relatively narrow range of WHSV studied in this work may also cause uncertainties.

The effect of WHSV on the reaction is shown in Figure 10. The results show that the deviation between experimental and calculated results for higher WHSV is more pronounced. The reason might be due to the relatively large experimental uncertainties at high WHSVs.

As can be seen from Figure 11, water is treated directly as a reactant and its influence on the product distribution can be

Figure 11. Comparison of the experimental and calculated mass fraction of each lump with time on stream: the effect of water. (A) $X_{w0} = 0.25$ and (B) $X_{w0} = 0$. Dots: Experiment; Lines: Calculation.

[Color figure can be viewed at wileyonlinelibrary.com]

well reproduced without introducing any extra correlations. The variation between experimental work and calculated results is quite small.

It should be noted that operating conditions have a great impact on the MTO reaction mechanism. For example, the active intermediate species might be totally different for different temperatures, and the amount of water in the feed and the WHSV might also influence the secondary reactions in the process. Therefore, the operating conditions in the current work were chosen carefully to cover the range of industrial operating conditions. In this regard, the application of the current model is limited to a relatively small range. Nevertheless, the model has been implemented in the simulations of DMTO reactors at different scales by incorporating a coke distribution model and a general fluidized bed reactor model. The simulation results show that the current model can provide a generic and robust way to well predict the methanol conversion and product distribution from laboratory scale reactor to industrial reactor. The details about model development and simulations of these reactors are the subject of a parallel publication.[53]

Conclusions

A kinetic model for MTO process has been established based on the dual-cycle reaction mechanism, which takes into consideration the autocatalytic nature of the reaction by adding two virtual lumps, that is, S and R, to account for the effect of olefins-based and aromatics-based catalytic cycle. Reactions in olefins-based cycle are assumed to occur on the active sites of catalyst surface, while aromatic species occupying these sites act as aromatics-based cycle. Gaseous species are assumed to be formed *via* both cycles separately. Compared to the direct methanol conversion, side reactions are less significant, and thus only the methylation of ethylene to propylene is considered in the current model.

Catalyst deactivation by coke deposition is also of great importance in MTO process. However, the active and deactivating species in MTO process are still ambiguous. Therefore, it is assumed that all the confined species are active species, and a phenomenological deactivation model is proposed to account for the difference between the coke and active species confined in the catalyst.

Kinetic parameters are estimated with experimental data from a laboratory scale fluidized bed reactor. Based on the simplified dual-cycle reaction mechanism, the initial and steady stage, as well as the deactivation process in MTO reaction could be quantified by the current model. The model is applied to simulate a laboratory scale MTO fluidized bed reactor, and it is shown that major features of MTO reaction can be well quantified. Then the model is used to simulate the DMTO reactors from pilot-scale to commercial scale. Good agreements between the simulation results and experimental data suggest that the current kinetic model is generic and robust in the design and operation optimization of industrial MTO fluidized bed reactors.

Acknowledgment

Literature Cited

1. Tian P, Wei Y, Ye M, Liu Z. Methanol to olefins (MTO): from fundamentals to commercialization. *ACS Catal*. 2015;5:1922-1938.
2. Chen NY, Reagan WJ. Evidence of autocatalysis in methanol to hydrocarbon reactions over zeolite catalysts. *J Catal*. 1979;59:123-129.
3. Ono Y, Mori T. Mechanism of methanol conversion into hydrocarbons over ZSM-5 zeolite. *J Chem Soc Farad Trans 1*. 1981;77:2209-2221.
4. Chang CD. Hydrocarbons from methanol. *Catal Rev*. 1983;25:1-118.
5. Kolboe S. Methanol reactions on ZSM-5 and other zeolite catalysts-autocatalysis and reaction mechanism. *Acta Chem Scand*. 1986;40: 711-713.
6. Kolboe S. On the mechanism of hydrocarbon formation from methanol over protonated zeolites. In: Methane Conversion, Bibby DM, Chang CD, Howe RF, Yurchak S, eds. *Studies in Surface Science and Catalysis, Vol* 36. Amsterdam: Elsevier, 1988:189-193.
7. Dessau RM, LaPierre RB. On the mechanism of methanol conversion to hydrocarbons over HZSM-5. *J Catal*. 1982;78:136-141.
8. Dessau RM. On the H-ZSM-5 catalyzed formation of ethylene from methanol or higher olefins. *J Catal*. 1986;99:111-116.
9. Mole T, Whiteside JA, Seddon D. Aromatic co-catalysis of methanol conversion over zeolite catalysts. *J Catal*. 1983;82:261-266.
10. Mole T, Bett G, Seddon D. Conversion of methanol to hydrocarbons over ZSM-5 zeolite: an examination of the role of aromatic hydrocarbons using ^{13}carbon- and deuterium-labeled feeds. *J Catal*. 1983;84.
11. Dahl I, Kolboe S. On the reaction mechanism for propene formation in the MTO reaction over SAPO-34. *Catal Lett*. 1993;20:329-336.
12. Dahl IM, Kolboe S. On the reaction mechanism for hydrocarbon formation from methanol over SAPO-34: I. Isotopic labeling studies of the co-reaction of ethene and methanol. *J Catal*. 1994;149:458-464.
13. Dahl IM, Kolboe S. On the reaction mechanism for hydrocarbon formation from methanol over SAPO-34: 2. Isotopic labeling studies of the co-reaction of propene and methanol. *J Catal*. 1996;161: 304-309.
14. Svelle S, Joensen F, Nerlov J, et al. Conversion of methanol into hydrocarbons over zeolite H-ZSM-5: ethene formation is mechanistically separated from the formation of higher alkenes. *J Am Chem Soc*. 2006;128:14770-14771.
15. Svelle S, Olsbye U, Joensen F, Bjorgen M. Conversion of methanol to alkenes over medium- and large-pore acidic zeolites: steric manipulation of the reaction intermediates governs the ethene/propene product selectivity. *J Phys Chem C*. 2007;111:17981-17984.
16. Bjørgen M, Svelle S, Joensen F, et al. Conversion of methanol to hydrocarbons over zeolite H-ZSM-5: on the origin of the olefinic species. *J Catal*. 2007;249:195-207.
17. Dai W, Wang C, Dyballa M, et al. Understanding the early stages of the methanol-to-olefin conversion on H-SAPO-34. *ACS Catal*. 2015;5: 317-326.
18. Wang CM, Wang YD, Xie ZK. Insights into the reaction mechanism of methanol-to-olefins conversion in HSAPO-34 from first principles: are olefins themselves the dominating hydrocarbon pool species? *J Catal*. 2013;301:8-19.
19. Wang CM, Wang YD, Xie ZK. Verification of the dual cycle mechanism for methanol-to-olefin conversion in HSAPO-34: a methylbenzene-based cycle from DFT calculations. *Catal Sci Technol*. 2014;4:2631-2638.
20. Hwang A, Prieto-Centurion D, Bhan A. Isotopic tracer studies of methanol-to-olefins conversion over HSAPO-34: the role of the olefins-based catalytic cycle. *J Catal*. 2016;337:52-56.
21. Park TY, Froment GF. Kinetic modeling of the methanol to olefins process. 1. Model formulation. *Ind Eng Chem Res*. 2001;40:4172-4186.
22. Park TY, Froment GF. Kinetic modeling of the methanol to olefins process. 2. Experimental results, model discrimination, and parameter estimation. *Ind Eng Chem Res*. 2001;40:4187-4196.
23. Kumar P, Thybaut JW, Svelle S, Olsbye U, Marin GB. Single-event microkinetics for methanol to olefins on H-ZSM-5. *Ind Eng Chem Res*. 2013;52:1491-1507.
24. Bos ANR, Tromp PJJ, Akse HN. Conversion of methanol to lower olefins. Kinetic modeling, reactor simulation, and selection. *Ind Eng Chem Res*. 1995;34:3808-3816.
25. Gayubo AG, Aguayo AT, Sánchez del Campo AE, Tarrío AM, Bilbao J. Kinetic modeling of methanol transformation into olefins on a SAPO-34 catalyst. *Ind Eng Chem Res*. 2000;39:292-300.
26. Gayubo AG, Aguayo AT, Alonso A, Atutxa A, Bilbao J. Reaction scheme and kinetic modelling for the MTO process over a SAPO-18 catalyst. *Catal Today*. 2005;106:112-117.
27. Gayubo AG, Aguayo AT, Alonso A, Bilbao J. Kinetic modeling of the methanol-to-olefins process on a Silicoaluminophosphate (SAPO-

18) catalyst by considering deactivation and the formation of individual olefins. *Ind Eng Chem Res*. 2007;46:1981-1989.

28. Ying L, Yuan X, Ye M, Cheng Y, Li X, Liu Z. A seven lumped kinetic model for industrial catalyst in DMTO process. *Chem Eng Res Des*. 2015;100:179-191.

29. Wu W, Guo W, Xiao W, Luo M. Dominant reaction pathway for methanol conversion to propene over high silicon H-ZSM-5. *Chem Eng Sci*. 2011;66:4722-4732.

30. Guo W, Wu W, Luo M, Xiao W. Modeling of diffusion and reaction in monolithic catalysts for the methanol-to-propylene process. *Fuel Process Technol*. 2013;108:133-138.

31. Wen M, Ding J, Wang C, et al. High-performance SS-fiber@HZSM-5 core–shell catalyst for methanol-to-propylene: a kinetic and modeling study. *Microporous Mesoporous Mater*. 2016;221:187-196.

32. Huang X, Aihemaitijiang D, Xiao WD. Co-reaction of methanol and olefins on the high silicon HZSM-5 catalyst: a kinetic study. *Chem Eng J*. 2016;286:150-164.

33. Huang X, Li H, Li H, Xiao WD. Modeling and analysis of the Lurgi-type methanol to propylene process: optimization of olefin recycle. *AIChE J*. 2017;63:306-313.

34. Wragg DS, O'Brien MG, Bleken FL, Di Michiel M, Olsbye U, Fjellvåg H. Watching the methanol-to-olefin process with time- and space-resolved high-energy operando X-ray diffraction. *Angew Chem Int Ed*. 2012;51:7956-7959.

35. Chen D, Grønvold A, Moljord K, Holmen A. Methanol conversion to light olefins over SAPO-34: reaction network and deactivation kinetics. *Ind Eng Chem Res*. 2007;46:4116-4123.

36. Westgård Erichsen M, Svelle S, Olsbye U. The influence of catalyst acid strength on the methanol to hydrocarbons (MTH) reaction. *Catal Today*. 2013;215:216-223.

37. Froment GF. Kinetic modeling of hydrocarbon processing and the effect of catalyst deactivation by coke formation. *Catal Rev Sci Eng*. 2008;50:1-18.

38. Arstad B, Kolboe S. Methanol-to-hydrocarbons reaction over SAPO-34. Molecules confined in the catalyst cavities at short time on stream. *Catal Lett*. 2001;71:209-212.

39. Fu H, Song W, Haw JF. Polycyclic aromatics formation in HSAPO-34 during methanol-to-olefin catalysis: ex situ characterization after cryogenic grinding. *Catal Lett*. 2001;76:89-94.

40. Song W, Fu H, Haw JF. Selective synthesis of methylnaphthalenes in HSAPO-34 cages and their function as reaction centers in methanol-to-olefin catalysis. *J Phys Chem B*. 2001;105:12839-12843.

41. Hereijgers BPC, Bleken F, Nilsen MH, et al. Product shape selectivity dominates the methanol-to-olefins (MTO) reaction over H-SAPO-34 catalysts. *J Catal*. 2009;264:77-87.

42. Olsbye U, Svelle S, Lillerud KP, et al. The formation and degradation of active species during methanol conversion over protonated zeotype catalysts. *Chem Soc Rev*. 2015;44:7155-7176.

43. Ying L, Ye M, Cheng YW, Li X. Characteristics of coke deposition over a SAPO-34 catalyst in the methanol-to-olefins reaction. *Pet Sci Technol*. 2015;33:984-991.

44. Geldart D. The effect of particle size and size distribution on the behaviour of gas-fluidised beds. *Powder Technol*. 1972;6:201-215.

45. Ying L, Ye M, Cheng Y, Li X, Liu Z. A kinetic study of methanol to olefins (MTO) process in fluidized bed reactor. In: JAM K, Mudde RE, van Ommen JR, Deen NG, eds. *The 14th International Conference on Fluidization – From Fundamentals to Products*. ECI Digital Archives; 2013.

46. Schulz H, Wei M. Pools and constraints in methanol conversion to olefins and fuels on zeolite HZSM5. *Top Catal*. 2013;57:683-692.

47. Wu X, Abraha MG, Anthony RG. Methanol conversion on SAPO-34: reaction conditions for fixed-bed reactor. *Appl Catal A*. 2004;260:63-69.

48. Chen D, Rebo HP, Grønvold A, Moljord K, Holmen A. Methanol conversion to light olefins over SAPO-34: kinetic modeling of coke formation. *Microporous Mesoporous Mater*. 2000;35–36:121-135.

49. Gayubo AG, Aguayo AT, Morán AL, Olazar M, Bilbao J. Role of water in the kinetic modeling of catalyst deactivation in the MTG process. *AIChE J*. 2002;48:1561-1571.

50. De Wispelaere K, Wondergem CS, Ensing B, et al. Insight into the effect of water on the methanol-to-olefins conversion in H-SAPO-34 from molecular simulations and in situ microspectroscopy. *ACS Catal*. 2016;6:1991-2002.

51. Shahda M, Dengchao Y, Huixin W. Methanol conversion to hydrocarbons over a SAPO-34 catalyst in a pulse micro reactor. *Pet Sci Technol*. 2008;26:1893-1903.

52. De Wispelaere K, Hemelsoet K, Waroquier M, Van Speybroeck V. Complete low-barrier side-chain route for olefin formation during methanol conversion in H-SAPO-34. *J Catal*. 2013;305:76-80.

53. Li H, Yuan X, Ye M, Liu Z. Study of catalyst coke distribution based on population balance theory: application to methanol to olefins process. *AIChE J*. Submitted for publication.